The University of Kiel (UNIK) Monte Carlo radiative transfer model

Andreas Macke and Ronald Scheirer

Institut für Meereskunde an der Universität Kiel
Düsternbrooker Weg 20
D-24105 Kiel, Germany
email: amacke@ifm.uni-kiel.de, rscheirer@ifm.uni-kiel.de

1 Introduction

The radiative transfer model at the Institute for Marine Research at the University Kiel (UNIK) is a forward Monte Carlo method. Its main purpose is to calculate domain-averaged solar radiative fluxes for 3d inhomogeneous cloudy atmospheres. The latter are mainly taken from cloud resolving atmospheric models and from cloud radar observations. The Monte Carlo results are used to parameterize broad band solar radiative fluxes in terms of bulk cloud properties like liquid and ice water path for use in large scale atmospheric models.

2 Model description

Free path lengths and scattering directions are simulated as outlined in (Marchuk et al., 1980) by random processes with Lamberts law of attenuation and the scattering phase function as the probability density functions for the free path length and the scattering direction. Absorption is taken into account by multiplying the incident photon weight with the particles' single scattering albedo.

The 3d model domain is divided into grid-boxes with indices (i, j, k) and geometrical dimensions $l_x(i)$, $l_y(j)$, and $l_z(k)$ along x-, y-, and z-direction. Each grid-box is characterized by a volume extinction coefficient $\beta(i, j, k)$, a scattering phase function $P(\theta, i, j, k)$ with scattering angle θ, and a single scattering albedo $\omega_0(i, j, k)$. These parameters are calculated by Mie-theory for water droplets and by geometric optics models for ice crystals, snow and graupel particles (Macke et al., 1996), and nonspherical raindrops (Macke and Grossklaus, 1998) for a wide range of wavelengths, particle sizes and shapes. Scattering and absorption at gas molecules are calculated line by line for predefined spectral intervals as described in (Scheirer and Macke, 2000).

The original photon position is uniformly distributed on the top layer $(i, j, k_{\max})$ of the model domain. Photons are traced from the starting point on one grid-box surface to the intersection with the nearest neighbour grid-box surface as illustrated in Fig. 1. This process is repeated l times until the cumulated optical thickness

$$\tau_{\text{cum}} = \sum_l \beta(i, j, k) t_l \qquad (1)$$

exceeds the randomly chosen (exponentially distributed) optical thickness τ_{rand}. The t_l denote the step lengths within the individual grid-boxes. Subsequently, the photon steps backward by

$$t_{back} = (\tau_{\text{cum}} - \tau_{\text{rand}})/\beta(i, j, k) \qquad (2)$$

to ensure that the total photon path exactly matches the τ_{rand}.

The scattering phase function is given in discrete steps with scattering angles θ_i and scattering phase function $P(\theta_i)$. The latter represents the average scattering phase function along a finite scattering

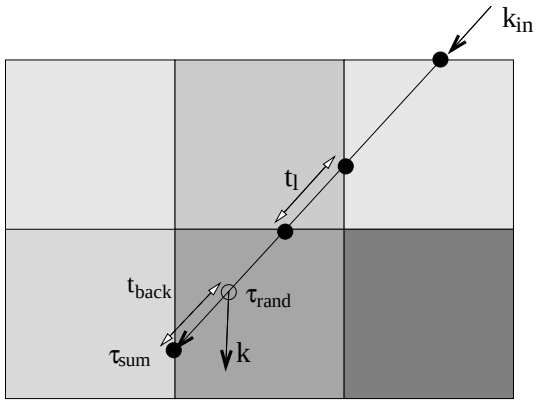

Figure 1: Illustration of photon tracing within a regular array of cloud boxes.

angle interval $[\theta_{i,min}, \theta_{i,max}]$ with center angle θ_i. The Monte Carlo procedure selects the scatterig angle index i according to

$$S_{i-1} < R < S_i \text{ with } S_i = \sum_{j=1}^{i} P(\theta_j)\Delta\Omega(\theta_j) \quad (3)$$

$\Delta\Omega(\theta_i)$ is the solid angle interval corresponding to $[\theta_{i,min}, \theta_{i,max}]$ and R denotes a random number uniformly distributed between 0 and 1. The exact scattering angle is then interpolated by

$$\theta = \theta_{i,min} + t \cdot \theta_{i,max} \quad \text{with} \quad t = \frac{R - S_{i-1}}{S_i - S_{i-1}} \quad (4)$$

The azimuth scattering angle ϕ is uniformly distributed between 0 and 2π. The new scattering direction $\underline{\mathbf{k}} = (k_x, k_y, k_z)$ is calculated from the previous direction and the zenith and azimuth scattering angles as described in (Marchuk et al., 1980), Chapter 2.2.

At each scattering process the photon energy E reduces to $E \cdot \omega_0$. The absorbed energy is $A = E(1 - \omega_0)$.

The energy of those photons leaving the cloud is stored into predefined solid angle intervals $\Delta\Omega(i,j)$, defined by a zenith-azimuth grid-box $[\theta_{i,min}, \theta_{i,max}] \times [\phi_{j,min}, \phi_{j,max}]$. Upward ($R$), downward ($T$), and absorbed ($A$) fluxes are calculated by adding up the corresponding photon energies. Net horizontal transport H is given by

$$H = I - R - T(1 - \alpha) - A, \quad (5)$$

where I is the incoming flux and α the surface albedo. Surface reflection is accounted for by

$$E \rightarrow E \cdot \alpha \quad (6)$$

$$(k_x, k_y, k_z) = (\sin\tilde{R}, \cos\tilde{R}, \cos^{-1} R^{\frac{1}{2}}), \quad (7)$$

whith $\tilde{R} = 2\pi R$. The radiances $I(i,j)$ along the direction of the solid angle interval $[\theta_{i,min}, \theta_{i,max}] \times [\phi_{j,min}, \phi_{j,max}]$ are calculated by

$$I(i,j) = \pi \frac{E(i,j)}{I\Delta\Omega(i,j)} \quad (8)$$

The statistical errors for fluxes and radiances are given by $1/\sqrt{n}$, where n is the number of photons collected into the corresponding 2d angular bins.

Radiance calculations for the cases defined in phase 1 of the 3d cloud intercomparison project have been performed for 2° by 2° angular bins.

3 Some Results

Most applications of the radiative transfer code so far have been performed for 3d cloud structures resulting from the non-hydrostatic mesoscale atmospheric model GESIMA (Eppel et al., 1995). An illustration of GESIMA output is shown in Fig. 2. Liquid water, snow, rain and ice may contribute to the total extinction and to the average scattering and absorption properties in each grid-box. Fig. 3 shows size distribution averaged scattering phase functions for various particle shapes and effective particle sizes as used in this study.

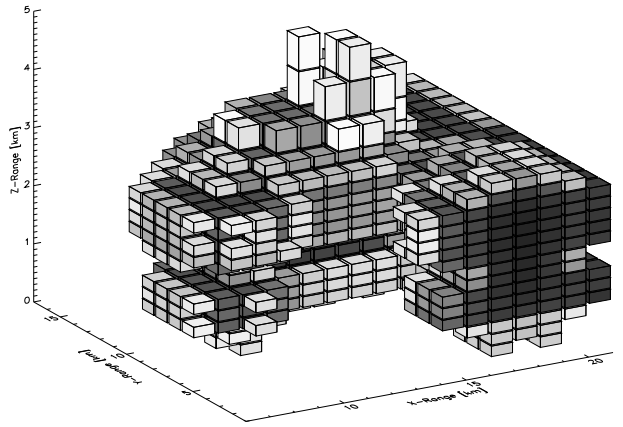

Figure 2: 3d clouds as realized by GESIMA. Darker boxes correspond to larger optical thickness. From (Scheirer and Macke, 2000).

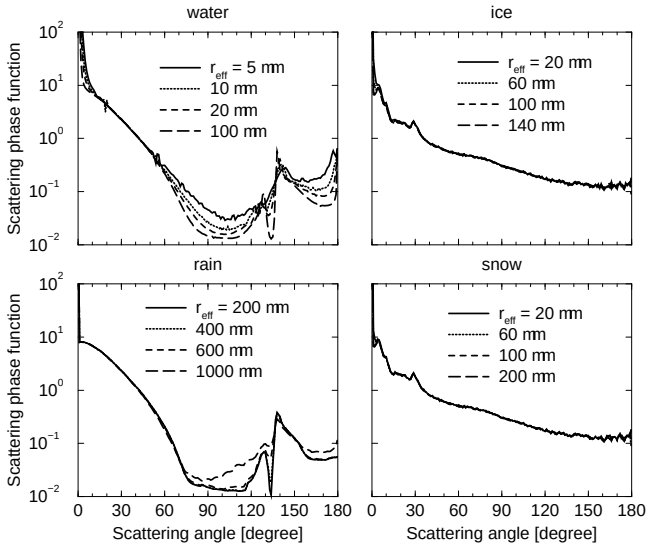

Figure 3: Phase functions at visible wavelengths for water droplets, rain drops, snow and ice crystals with different effective radii.

As an example result, Fig. 4 shows the albedo differences between 3d clouds with prevailing liquid water and plane-parallel homogeneous water clouds with same optical thickness (left) and same total water path (right). The Monte Carlo calculations for the 3d clouds have been performed with horizontally periodic boundary conditions. The aalbedo bias is stronger pronounced for summertime convective cloud scenarios (I, IV) than for stratiform clouds (II,III). The stratiform wintertime cloud (II) shows a smaller bias than the summertime cloud (III) because it contains larger portions of the more isotropically scattering ice and snow particles. For the same reason, the albedo differences occasionally becomes positive for the 3d clouds. For a given cloud type, the albedo bias is correlated with cloud optical thickness which may render possible an albedo correction of radiative transfer results that are based on the idealised 1d cloud geometries. Not surprisingly, the albedo-bias is much less significantly correlated to total cloud water path than to optical thickness. Therefore, realistic correlations between optical thickness and water contents for different cloud situations are required for parameterizing radiative fluxes and radiances in terms of bulk cloud properties.

4 Suggestions for future work

3d cloud inhomogeneities are caused by variations in both the cloud volume extinction coefficient and the scattering and absorption properties of the cloud particles. Even for water clouds, changes in effective droplet size may have a noticeable effect on the radiance fields. However, the effect is stronger for both radiances and fluxes for mixed phase and cirrus clouds. Except for low-level summer time clouds, water and ice phase usually co-exist in a cloudy atmospheric column. We therefore propose to define cloud cases for future 3d cloud intercomparisons where

1) spatial variations of scattering and absorption properties are accounted for, and

2) highly anisotropic scattering phase functions like those for ice and snow particles are applied.

The first point can be achieved by applying results from spectral (in terms of size distributions) cloud resolving models to the radiative transfer

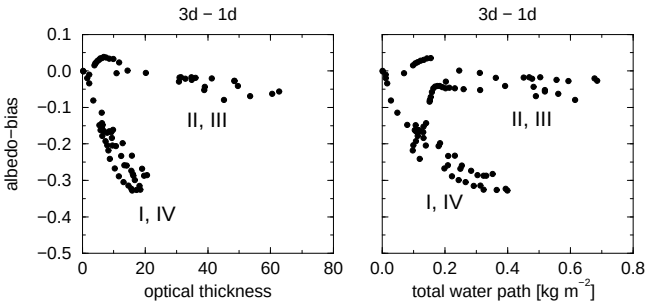

Figure 4: Albedo differences as a function of optical thickness and total water path between inhomogeneous mixed phase clouds (3d) with dominant liquid phase and plane parallel homogeneous water clouds with prescribed scattering properties (1d). From Macke et al. (1999).

codes. Appropriate candidates for point 2) may be phase functions for regular hexagonal ice columns (Takano and Liou, 1989) and for irregular shaped polycrystals (Macke et al., 1996). The latter may also be representative for snow and graupel- particles in mixed-phase clouds.

References

Eppel, D. P., Kapitza, H., Clausen, M., Jacob, D., Koch, W., Levkov, W., Mengelkamp, H.-T., and Werrmann, N. (1995). The nonhydrostatic mesoscale model GESIMA. Part II: Parameterizations and applications. *Contr. Atmos. Phys.* **68**, 15–41.

Macke, A., and Grossklaus, M. (1998). Light scattering by nonspherical raindrops: implications for lidar remote sensing of rainrates. *J. Quant. Spectros. Radiat. Transfer* **60**, 355–363.

Macke, A., Mitchell, D., and von Bremen, L. (1999). Monte carlo radiative transfer calculations for inhomogeneous mixed phase clouds. *Phys. Chem. Earth (B)* **24**, 237–241.

Macke, A., Mueller, J., and Raschke, E. (1996). Single scattering properties of atmospheric ice crystals. *J. Atmos. Sci* **53**, 2813–2825.

Marchuk, G. I., Mikhailov, G. A., Nazareliev, R. D., Darbinjan, R. A., Kargin, B. A., and S., E. B. (1980). The Monte Carlo Methods in Atmospheric Optics. Springer-Verlag.

Scheirer, R., and Macke, A. (2000). Influence of the gasous atmosphere on solar fluxes of inhomogeneous clouds. *Phys. Chem. Earth (B)* **25**, 73–76.

Takano, Y., and Liou, K. N. (1989). Solar radiative transfer in cirrus clouds, part I: Single-scattering and optical properties of hexagonal ice crystals. *J. Atmos. Sci* **46**, 3–18.